BIOCELL

Tech Science Press

http://doi.org/10.32604/biocell.2026.076001

ARTICLE

miR-216a-5p Improves Macrophage M1 Polarization and Pyroptosis in URSA via Modulating HMGB1 to Regulate TLR4/NF-κB/NLRP3 Axis

Weina Xu[1], Yi Xia[1], Qing Shen[1], Ling Ai[1] and Yingye Lu[2,*]

[1]Department of Obstetrics, Jiaxing Maternity and Child Health Care Hospital, Jiaxing, China
[2]Department of Traditional Chinese Medicine, Jiaxing Maternity and Child Health Care Hospital, Jiaxing, China
*Corresponding Author: Yingye Lu. Email: 18324351140@163.com

Received: 12 November 2025; Accepted: 27 February 2026; Published: 09 June 2026

ABSTRACT: Background: Dysfunction of decidual macrophages (dMφ) mediated by high mobility group box 1 (HMGB1) is related to unexplained recurrent spontaneous abortion (URSA), but its upstream regulatory mechanism remains unclear. The research explores whether miR-216a-5p regulates the toll-like receptor 4/nuclear factor-κB/nucleotide-binding oligomerization domain-like receptor protein 3 (TLR4/NF-κB/NLRP3) signaling axis by targeting HMGB1, thereby affecting the M1 polarization and pyroptosis of dMφ in URSA. **Methods:** The URSA mouse model was established, and primary dMφ was isolated and cultured. HMGB1 and miR-216a-5p were overexpressed or knocked down. Their expressions were examined. Their targeting relationship was verified through a bioinformatics database and dual luciferase assays. Immunofluorescence and Western blot detected macrophage M1/M2 phenotype and key indicators of pyroptosis. The TLR4/NF-κB/NLRP3 signal was evaluated. Additionally, HE staining was used to evaluate the tissue damage of the maternal-fetal interface (MFI). **Results:** HMGB1 was enhanced, and miR-216a-5p was decreased within URSA mice. Overexpression of HMGB1 aggravated the inflammatory injury of decidual tissue in URSA mice, increased M1 macrophage proportion, and activated the TLR4/NF-κB/NLRP3 signal and pyroptosis pathway. miR-216a-5p inhibited HMGB1 expression, and its overexpression significantly reversed the above pathological changes, including reducing decidual inflammatory injury, inhibiting macrophage M1 polarization and pyroptosis, and inhibiting TLR4/NF-κB/NLRP3 signal. **Conclusion:** miR-216a-5p inhibited TLR4/NF-κB/NLRP3 signal by targeting HMGB1, reduced M1 polarization and pyroptosis of dMφ, and alleviated inflammatory damage at the MFI of URSA. This finding offers novel bases for the mechanism study and targeted therapy of URSA.

KEYWORDS: miR-216a-5p; high mobility group box 1; decidual macrophages; unexplained recurrent spontaneous abortion

1 Introduction

Globally, 1%–5% of women have recurrent spontaneous abortion (RSA) during their reproductive years [1]. The causes of RSA are very complex. Previous etiological studies mainly focused on chromosomal factors, abnormal uterine anatomy, endocrine abnormalities, thrombosis tendency, immune dysfunction, etc. However, after excluding the above common factors, RSA without identifiable causes is called unexplained recurrent spontaneous abortion (URSA) [2], and there is still no clear treatment for URSA.

Existing studies have gradually revealed that impaired immune tolerance at the maternal-fetal interface (MFI) is a significant mechanism underlying URSA [3]. Decidual tissue contains a large number of pregnancy-related immune cells, including macrophages [4,5]. It plays an indispensable role in decidual macrophages (dMφ) in maintaining maternal-fetal immune balance and promoting embryo implantation and development.

In early pregnancy, dMφ accounts for about 20% of decidual leukocytes, which is the second largest number of leukocytes at the MFI [6]. Under physiological conditions, dMφ participates in pregnancy regulation by dynamically regulating M1/M2 phenotypic balance. In the implantation, the M1 type is dominant, while after attachment and invasion of trophoblast cells, it is transformed into the M2 type. Subsequently, she recovered to M1 type during delivery. In MFI of URSA, the M1/M2 phenotype balance was broken, which was manifested as an enhancement in M1 macrophage proportion and an enhancement in the ratio of M1/M2. This imbalance may lead to a shift in the immune microenvironment to the pro-inflammatory direction, resulting in an immune attack on the embryo, thereby increasing the risk of miscarriage [7,8]. The proportion of M1 pro-inflammatory macrophages in URSA decidual tissues was significantly increased, accompanied by inflammatory factor release, which directly destroyed the homeostasis of MFI [6,9]. Therefore, any abnormalities in the dMφ phenotype may adversely affect pregnancy outcomes, resulting in complications (preeclampsia, preterm birth, and URSA) [10].

High mobility group box 1 (HMGB1) is crucial for pregnancy. HMGB1 level in serum and decidual tissue of URSA patients is significantly increased, and it is positively correlated with abortion risk [11]. Mechanistically, HMGB1 can activate toll-like receptor 4 (TLR4), leading to nuclear factor-κB (NF-κB) activation, promote inflammatory factor release, and participate in the URSA pathological process. Notably, aspirin (ASPL), as an anti-inflammatory drug, reduces HMGB1 levels in URSA. In addition, recent studies have further revealed that HMGB1 secreted by macrophages can activate pyroptosis by the TLR/NF-κB axis, causing inflammation and promoting URSA progression [12]. This suggests that HMGB1 can be used as an important target for improving URSA.

Pyroptosis occurs mainly in phagocytic cells and is vital for regulating the URSA immune microenvironment [13,14]. Nucleotide-binding oligomerization domain-like receptor protein 3 (NLRP3) inflammasome is a key mediator of macrophage pyroptosis. Its activation can promote cysteinyl aspartate-specific proteinase-1 (Caspase-1) cleavage and Gasdermin D (GSDMD) pore formation, causing cytokine release and cell rupture [15]. NLRP3 and Caspase-1 expressions were markedly enhanced, suggesting that abnormal activation of the pyroptosis pathway is closely related to URSA [8]. HMGB1 induces pyroptosis via promoting NLRP3 inflammasome assembly, causing MFI destruction [12]. Therefore, the HMGB1-TLR4/NF-κB/NLRP3 axis constitutes a complete signaling cascade from the initiation of inflammatory signals to the execution of pyroptosis, jointly exacerbating the damage of MFI.

In addition to protein molecules, non-coding RNAs, especially microRNAs (miRNAs), have been vital for regulating pregnancy immunity in recent years. miR-194-5p inhibits NF-κB signal, and then regulates the apoptosis of M1 macrophages to participate in the pathogenesis of URSA [16], suggesting that miRNA-mediated macrophage function regulation is an important molecular mechanism of URSA. Among many miRNAs, this study focused on miR-216a-5p. Although there is no report that it is directly associated with URSA, it has been shown in other inflammation-related diseases to reduce inflammation through the HMGB1/TLR4/NF-κB axis [17]. It inhibited the TLR4/NF-κB axis and alleviated inflammatory response [18]. Moreover, the miR-216a-5p/HMGB1 axis participates in regulating macrophage polarization [19]. In addition, it was also found to regulate NLRP3-mediated pyroptosis and myocardial cell injury [20]. Thus, miR-216a-5p may be located upstream within HMGB1-TLR4/NF-κB/NLRP3 signaling and become a hub regulatory molecule that connects macrophage phenotypic polarization and pyroptosis. However, whether and how this molecule regulates macrophage function and MFI homeostasis in URSA through this axis is still unknown.

Based on the above research background, this study hypothesized that in URSA, miR-216a-5p suppresses the TLR4/NF-κB/NLRP3 axis by targeting HMGB1, thereby reducing M1 polarization and pyroptosis of dMφ.

To verify this hypothesis, this study will use URSA model mice to clarify miR-216a-5p expressions in URSA decidual tissue, verify its targeted regulation relationship with HMGB1, and clarify the functional mechanism within the HMGB1-TLR4/NF-κB/NLRP3 signal that affects the M1 polarization and pyroptosis of dMφ. Our research aims to provide novel theoretical bases for investigating URSA pathogenesis and develop potential molecular targets for its clinical targeted therapy.

2 Methods

2.1 URSA Mouse Model

The animal experiments were approved by the Jiaxing Maternity and Child Health Care Hospital Ethics Committee (No. KY-2025-129). At the age of 8 weeks, 132 CBA/J female mice, 60 DBA/2J male mice, and 12 BALB/c male mice were purchased from Huafukang Company (Beijing, China), a total of 204 mice. All mice were housed in an SPF animal room with 22°C and 50% relative humidity to simulate normal circadian rhythms. The mice could eat and drink freely, change the padding regularly, and clean the cage. The experimental process strictly abides by the 3R principle of substitution, reduction, and optimization.

All female mice were randomly divided into 6 groups. Sample size estimation: Using G*Power (version 3.1.9.7, Heinrich-Heine-Universität Düsseldorf, Düsseldorf, Germany), with Cohen's f = 0.4, $\alpha = 0.05$, 1-$\beta = 0.8$, and the sample size of each group was 7. The normal (NP) group was 22 CBA/J female mice mated with 12 BALB/c male mice. In the URSA group, 22 CBA/J female mice were mated with 12 DBA/2J male mice. The 22 CBA/J female mice treated with rhHMGB1 were mated with 12 DBA/2J male mice in the URSA+rhHMGB1 group. 22 CBA/J female mice treated with ASPL were mated with 12 DBA/2J male mice in the URSA+ASPL group. CBA/J female mice in the URSA+ASPL group were given drinking water containing ASPL (30 μg/mL, HY-14654, MedChemExpress, Monmouth Junction, NJ, USA) 7 days before mating and 7 days after vaginal plug. CBA/J female mice in the URSA+rhHMGB1 group were intraperitoneally injected with 50 μg/kg rhHMGB1 (H4652, Sigma, St. Louis, MO, USA) once every 2 days. CBA/J female mice in URSA+rhHMGB1+mimic-NC and URSA+rhHMGB1+mimic groups were injected with 20 nmol/100 μL mimic-NC and mimic-miR-216a-5p (GenePharma, Suzhou, China) by tail vein once every 3 days. To successfully mate, during the estrus of the female mice, the male and female were caged at night according to the ratio of 2:1, and the vaginal plug was examined at 7: 00–9: 00 the next morning. The female mice with vaginal plugs were recorded as day 0 of pregnancy. Considering that some mice were found to have clear vaginal plugs in the pre-experiment but were not pregnant at 11 days of pregnancy, 10–12 female mice with vaginal plugs were enrolled in each group in this part, ensuring there were 7 pregnant mice for final observation and analysis. On the 14th day of pregnancy, the mice were sacrificed, and the decidual tissue containing the embryo attachment point was quickly dissected. All subsequent histopathological analysis, molecular biological detection, and data statistics were performed by experimental personnel who were unaware of the grouping information of this study to ensure the objectivity of the results evaluation.

2.2 Hematoxylin and Eosin (HE) Staining

The mouse uterine decidual tissue was dehydrated by gradient ethanol (concentration of 70%, 80%, 90%, 95%, and 100%), transparentized by xylene (100%), embedded in paraffin, and serially sectioned by a microtome (RM2255, Leica, Nussloch, Germany) with a thickness of about 3 μm. Subsequently, HE staining was performed. The steps included 1% hematoxylin staining for 5 min, 0.5% eosin staining for 2 min, and neutral gum sealing. The sections were examined using a microscope (BX53, Olympus, Tokyo, Japan),

focusing on typical pathological changes of inflammatory injury such as inflammatory cell infiltration and cell disorder, and collecting images for subsequent analysis.

2.3 Isolation of dMφ from URSA Mice

The decidual tissues of 7 mice in the URSA group were collected and cut into pieces in 1× phosphate-buffered saline (PBS, pH 7.4), and DMEM/F12 medium (HY-K3002, MedChemExpress) containing 2 mg/mL collagenase IV and 100 U/mL DNase I was added. The digestion was performed at 37°C for 30 min until most of the tissue blocks were digested into single cell suspensions. Subsequently, the cells were initially isolated using Percoll density gradient centrifugation. The single cell suspension obtained after digestion and filtration was slowly added to the pre-prepared discontinuous Percoll gradient solution (the gradient was composed of 60%, 40%, and 20% Percoll solution from bottom to top, and each solution was diluted with 1× PBS to the corresponding volume ratio and adjusted to isotonic). Centrifugation was performed at 4°C for 20 min with a centrifugal force of 400× *g*. After centrifugation, the cell layer between the 40%–60% Percoll solution interface was carefully collected. The collected cells were added with excessive PBS, and centrifuged at 4°C, 300× *g* for 10 min. The process was repeated twice to completely remove the residual Percoll. Finally, the cell precipitate was resuspended for subsequent use. In order to obtain high-purity dMφs, the cells (1×10^8/mL) were incubated with $CD11b^+$ (8802-6860-74, Invitrogen, Carlsbad, CA, USA) immunomagnetic beads at 4°C for 20 min. Finally, the cells were loaded onto the LS sorting column (130-042-401, Miltenyi Biotec, Bergisch Gladbach, Germany), placed in the magnetic field to collect the magnetically labeled $CD11b^+$ cells, and the sorted cells were resuspended for subsequent culture or analysis. At least three independent biological replicates (n = 3) were performed for dMφ isolation and subsequent *in vitro* functional experiments.

2.4 Cell Grouping and Processing

GenePharma (Shanghai, China) was commissioned to construct the following plasmids and complete lentiviral packaging: miR-216a-5p inhibitor (inhibitor-miR-216a-5p) and its negative control (inhibitor-NC), miR-216a-5p mimics (mimics-miR-216a-5p) and its negative control (mimics-NC), HMGB1 overexpression vector (OE-HMGB1) and its negative control (OE-NC), and HMGB1 coding sequence expression vector without 3'UTR (pHMGB1-NoUTR). Lipofectamine^{TM}3000 (L3000150, Invitrogen, Carlsbad, CA, USA) kit was used to transfer HMGB1 overexpression plasmid (OE-HMGB1 group) and negative control OE-NC (OE-NC group), miR-216a-5p inhibitor (inhibitor-miR-216a-5p group) and negative control inhibitor-NC (inhibitor-NC group), miR-216a-5p mimics (mimics group) and negative control mimics-NC (mimics-NC group) specific for HMGB1 and miR-216a-5p into dMφ. The mimics-miR-216a-5p+pHMGB1-NoUTR co-transfection group was established to overexpress miR-216a-5p while forcing HMGB1 protein that was not regulated by its target. The operation steps were carried out according to the kit instructions. After 24 h, HMGB1 protein and miR-216a-5p levels were detected, so as to verify the transfection efficiency. After dMφ transfection, TLR4 agonist LPS and inhibitor TAK-242, NLRP3 agonist Nigericin (Nig), and inhibitor MCC950 were used to intervene. dMφ was treated with 1 mM TAK-242 (HY-11109, MedChemExpress) for 48 h, 100 ng/mL LPS (HY-D1056, MedChemExpress) for 5 h, 20 μM Nig (HY-127019, MedChemExpress) for 30 min, and 10 μM MCC950 (HY-12815, MedChemExpress) for 1 h, respectively.

Raw264.7 cells were purchased from Procell (CL-0190, Wuhan, China). After the cell line was purchased, it was identified by short tandem repeat (STR) to confirm its identity, and it was regularly tested to confirm that it was free of mycoplasma contamination. Raw264.7 cells were transfected with NC or OE-HMGB1 for 24 h, and then treated with LPS (100 ng/mL) and IFN-γ (20 ng/mL) for 24 h.

2.5 Enzyme-Linked Immunosorbent Assay (ELISA)

Inducible nitric oxide synthase (iNOS), interleukin (IL)-1β, IL-18, and tumor necrosis factor-α (TNF-α) kits were obtained from Elabscience (E-EL-M0696, E-EL-M0037, E-EL-M0730, E-EL-M3063, Wuhan, China). The decidual tissue of mice was added to PBS and fully ground on ice. dMφ were resuspended with 1× PBS (pH 7.4), and sonicated under ice bath conditions (output power 30%, pulse cycle: working 2 s/interval 3 s, total duration 60 s). The lysate was centrifuged at 4°C, 12,000× *g* for 5 min, and the supernatant was taken. Standard curves were constructed using known concentrations, with optical density (OD) values measured and plotted. Sample concentrations were subsequently calculated by comparing their OD readings against this reference curve.

2.6 Flow Cytometry Experiment

Mouse decidual tissues were digested with DMEM/F12 medium containing collagenase and DNase for 30 min. The cells were filtered and collected, and resuspended in 1× PBS (pH 7.4). Cells were blocked with Fc receptor blockers (422302, BioLegend, San Diego, CA, USA) to reduce non-specific staining. APC-CD11c (E-AB-F0991E, Elabscience) and FITC-CD206 (E-AB-F1135C, Elabscience) antibodies were added for fluorescence staining, and an isotype antibody control was set to ensure the accuracy of the results. Flow cytometry (Attune NxT, Thermo Fisher Scientific, Waltham, MA, USA) was used for detection. The $CD11c^{+}CD206^{-}$ cell population was defined as M1 macrophages. The level of apoptosis was detected by an apoptosis kit (E-CK-A217, Elabscience). The cells were incubated with 5 μL PI and 5 μL Annexin V-APC for 15 min, and analyzed by flow cytometry. For pyroptosis detection, cells were incubated with Alexa Fluor 488-labeled FLICA Caspase-1 (ICT098, ImmunoChemistry, Bloomington, MN, USA) probes for 1 h, and then fixed with 4% paraformaldehyde. To detect the characteristics of DNA breakage at the end of pyroptosis, TMR-labeled *In-Situ* Cell Death Detection reagent (12156792910, Roche Applied Science, Indianapolis, IN, USA) was used to label the cells. After all staining, flow cytometry was used for detection. The double-positive cells of Caspase-1 and TUNEL were considered to be pyroptosis cells.

dMφ was incubated with FITC-F4/80 (E-AB-F0995C, Elabscience), PE-CD86 (E-AB-F0994D, Elabscience), APC-CD86 (E-AB-F0994E, Elabscience), FITC-CD206 (E-AB-F1135C, Elabscience), PE-CD206 (E-AB-F1135D, Elabscience), PE-CD80 (E-AB-F0992D, Elabscience) antibodies for 30 min, and the isotype antibody control was set to ensure the accuracy of the results. After that, flow cytometry was used for detection.

2.7 PI Staining

10 μg/mL Hoechst 33342 dye (H3570, Thermo Fisher Scientific) was added to dMφ and incubated for 15 min, so that the dye could penetrate the cell membrane of all cells and label the nucleus. Subsequently, PI dye was added to continue incubation for 10 min, and observed using a fluorescence microscope (Nikon Eclipse C1, Nikon, Tokyo, Japan).

2.8 Immunofluorescence

The dMφ and mouse decidual tissue were fixed with 4% paraformaldehyde and blocked with 10% goat serum for 30 min. iNOS (ab178945, 1:500, Abcam, Cambridge, UK), F4/80 (ab300421, 1:50, Abcam), apoptosis-associated speck-like protein containing CARD (ASC, ab175449, 1:200, Abcam), CD68 (ab283654, 1:50, Abcam), CD206 (DF4149, 1:500, Affinity, Jiangsu, China), HMGB1 (ab79823, 1:250, Abcam), and TLR4 (AF7017, 1:500, Affinity) antibodies were incubated overnight at 4°C. After that, fluorescent antibody IgG (Goat Anti-Rabbit IgG H&L (Alexa Fluor® 488), ab150077, 1:1000, Abcam) was incubated for 2 h. Finally,

1 μg/mL 4′,6-diamidino-2-phenylindole (DAPI) solution was added for staining the nucleus. The slides were dried. The slides were observed under a fluorescence microscope.

The paraffin sections of mouse decidual tissue were dewaxed, repaired with 20 μg/mL protease K solution, and ruptured with membrane-breaking solution. The terminal deoxynucleotidyl transferase dUTP nick-end labeling (TUNEL) reaction solution was prepared according to the TUNEL kit (G1504, Servicebio, Wuhan, China), added dropwise to the sections, and incubated with the TUNEL reaction solution for 1 h. After the TUNEL reaction, 10% goat serum was added to block the sections, and then CD68 (ab283654, 1:50, Abcam) antibody was added to incubate overnight at 4°C. The next day, the fluorescent secondary antibody (Goat Anti-Rabbit IgG H&L (Alexa Fluor® 488), ab150077, 1:1000, Abcam) was added dropwise and incubated for 2 h. The staining was observed under a fluorescence microscope.

2.9 Reverse Transcription Quantitative Polymerase Chain Reaction (RT-qPCR)

RNAiso Plus reagent (9108Q, TaKaRa, Kusatsu, Japan) was used to extract total RNA from dMφ, and RNA concentration and purity were determined by ultramicro nucleic acid protein analyzer (Q5000, Quawell, San Jose, CA, USA). The PrimeScript™ FAST RT reagent Kit (RR092S, TaKaRa, Kusatsu, Japan) was employed for cDNA synthesis. Following this, qPCR amplification was conducted on a PCR instrument (ABI7500, Applied Biosystems, Foster City, CA, USA) using the qPCR kit (CN830S, TaKaRa, Kusatsu, Japan). U6 was the internal reference gene. The gene expressions were analyzed through the $2^{-\Delta\Delta CT}$ method. The primer sequences: U6: F: GGAACGATACAGAGAAGATTAGC, R: TGGAACGCTTCACGAATTTGCG; miR-216a-5p: F: TAATCTCAGCTGGCAACT, R: GGTGTCGTGGAGTCG.

2.10 Western Blot

Mouse decidual tissue was quickly thawed, and dMφ and Raw264.7 cells in each group were collected and homogenized with RIPA lysate containing protease inhibitors (G2002, Servicebio) to lyse cells and tissues. Using a high-speed refrigerated centrifuge (Centrifuge 5424R, Eppendorf, Hamburg, Germany), centrifuged at 4°C, 12,000× *g* for 15 min, the supernatant contained the total protein. Then the protein was quantified by the BCA kit (G2026, Servicebio), and the corresponding sample volume was calculated. After protein denaturation, an SDS-PAGE gel was prepared. After gel electrophoresis separation, the protein was transferred to a polyvinylidene difluoride (PVDF) membrane. The PVDF membrane was blocked with blocking solution (5% skim milk powder) for 90 min, incubated with primary antibodies (Table 1), and slowly shaken overnight in a refrigerator at 4°C. Tris-buffered saline with Tween 20 (TBST) was used to clean the protein bands, and the bands were incubated with secondary antibody for 2 h. The enhanced chemiluminescence (ECL) luminescent chromogenic solution (G2161, Servicebio) was added dropwise. The gel imaging system (Chemi Doc XRS, Bio-Rad, Hercules, CA, USA) was used to take pictures. The gray values of protein were tested using ImageJ software (1.53t, National Institutes of Health, Bethesda, MD, USA).

Table 1: The primary antibodies used for Western blot.

Protein Name	Dilution Ratio	Catalog Number	Producer
HMGB1	1:10,000	ab79823	Abcam
TLR4	1:2000	AF7017	Affinity
NF-κB	1:2000	AF5006	Affinity
p-NF-κB	1:2000	AF2006	Affinity
iNOS	1:1000	ab178945	Abcam
Arginase 1 (Arg1)	1:5000	ab124917	Abcam
NLRP3	1:1000	ab270449	Abcam

Table 1: *Cont.*

Protein Name	Dilution Ratio	Catalog Number	Producer
pro-Caspase-1	1:1000	ab179515	Abcam
Cleaved-Caspase-1	1:2000	AF4005	Affinity
pro-IL-1β	1:1000	WL02257	Wanleibio
Cleaved-IL-1β	1:2000	AF4006	Affinity
GSDMD	1:1000	ab219800	Abcam
Cleaved-GSDMD	1:1000	ab255603	Abcam
ASC	1:1000	ab309497	Abcam
IκB	1:5000	ab76429	Abcam
p-IκB	1:10,000	ab133462	Abcam
GAPDH	1:50,000	AF0911	Affinity

2.11 Dual Luciferase Assay

When dMφ cells were cultured to about 60% of the cells, Lipofectamine 3000 transfection reagent (L3000-015, Thermo Fisher Scientific) was used to transfect the HMGB1 wild-type reporter gene vector (WT-HMGB1), mutant reporter gene vector (MUT-HMGB1), and mimic-NC or mimic into the cells according to the instructions. After 48 h of transfection, the medium was discarded. Subsequently, following the dual luciferase reporter gene assay kit (E1910, Promega, Madison, WI, USA), lysis buffer was added to the cells to lyse them, and the lysis buffer was collected. The firefly luciferase detection substrate and the renilla luciferase detection substrate (pRL-TK, Promega) were added in turn, and the luciferase activity was measured. The relative activity of firefly luciferase was calculated by using Renilla luciferase activity as an internal reference.

2.12 Bioinformatics Analysis

The potential target genes of miR-216a-5p were analyzed by TargetScan (https://www.targetscan.org/vert_80/), miRWalk (http://mirwalk.umm.uni-heidelberg.de/), and miRTarBase (https://mirtarbase.cuhk.edu.cn/~miRTarBase/miRTarBase_2022/php/index.php) database. After obtaining the prediction results from each database, the online tool Venny (https://bioinfogp.cnb.csic.es/tools/venny/) analyzed the intersection of the three groups of gene lists and drew the Venn diagram to screen out the common candidate target genes.

2.13 Statistical Analysis

Statistical analysis was conducted using SPSS version 27.0 (SPSS Inc., Chicago, IL, USA). The sample size (n) of each group of data was clearly marked in the legends. The normality and variance homogeneity of all data were verified before analysis. Statistical differences among groups were assessed by one-way ANOVA with Tukey's post hoc test. Data are presented as the mean ± standard deviation, and significance was set at $p < 0.05$.

3 Results

3.1 HMGB1 Induced MFI Damage by Affecting M1 Polarization and Pyroptosis of dMφ in URSA Mice

The cells of uterine decidual tissue in normal mice were closely arranged in a mosaic shape, the cytoplasm was uniformly stained red, the nucleus showed a typical oval structure, the nucleolus was obvious and stained blue-purple, and the vascular endothelial structure was intact. The decidual tissue of URSA mice showed significant pathological changes of inflammatory injury, which were manifested as loose and disordered cell arrangement, obvious cytoplasmic edema, increased cell density, and accompanied

by a large number of inflammatory cell infiltration. Further intervention experiments showed that exogenous rhHMGB1 intervention aggravated the degree of inflammatory injury of URSA mice. After APSL intervention, the histological characteristics of the decidua were significantly improved, the cell morphology tended to be regular, and inflammatory cell infiltration was significantly lessened (Fig. 1A,B). iNOS$^+$F4/80$^+$ positive cell density in decidual tissue of URSA mice increased significantly, suggesting that local M1 macrophage numbers were enhanced (Fig. 1C,D). iNOS, IL-1β, and TNF-α contents were significantly enhanced within URSA mice (Fig. 1E–G). This indicated that inflammation and macrophage inflammatory activity were parallel in URSA mice. In addition, the percentage of M1 macrophages (CD11c$^+$CD206$^-$) and apoptotic cells (Annexin V$^+$PI$^+$) in decidual tissues of URSA mice was significantly increased by flow cytometry (Fig. 1H–K). Pyroptosis-specific detection further confirmed that the proportion of Caspase-1$^+$TUNEL$^+$ cells of URSA mice was markedly enhanced, and the number was also markedly increased (Fig. 1L,M). It is worth noting that rhHMGB1 treatment aggravated the above-mentioned macrophage polarization abnormalities and pyroptosis, while APSL intervention could effectively reverse the status of macrophage M1 polarization and pyroptosis within decidual tissues (Fig. 1H–M). In summary, HMGB1 induced MFI inflammatory damage by aggravating M1 polarization and pyroptosis of dMφ in URSA mice.

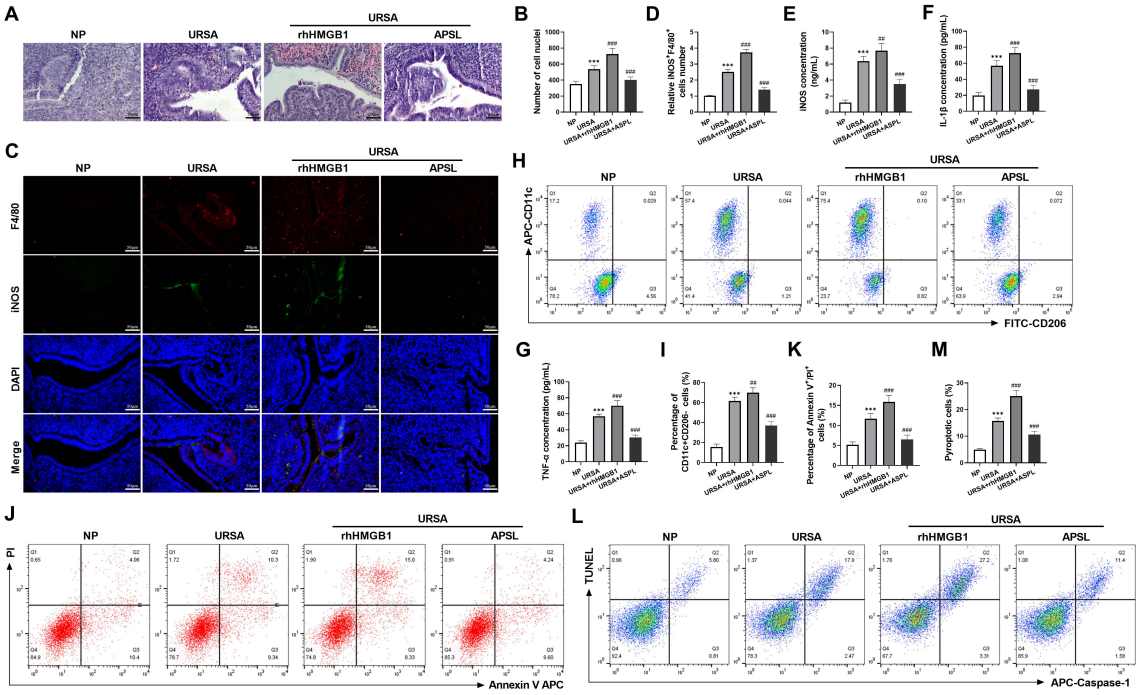

Figure 1: HMGB1 induced MFI damage by affecting M1 polarization and pyroptosis of dMφ in URSA mice. (**A**,**B**) HE staining observed decidual tissue inflammatory injury in mice. Cell density of decidual tissue in URSA mice increased, accompanied by a large number of inflammatory cell infiltrations (×40, 50 μm). (**C**,**D**) Local M1 macrophages (iNOS$^+$F4/80$^+$) within decidual tissue were detected by immunofluorescence, which was significantly increased in URSA mice and after rhHMGB1 intervention (×40, 50 μm). (**E**–**G**) iNOS, IL-1β, and TNF-α contents within decidual tissues were measured through ELISA, which were significantly increased in URSA mice and after rhHMGB1 intervention. (**H**,**I**) The proportion of M1 dMφ (CD11c$^+$CD206$^-$) in decidual tissue was measured using flow cytometry, which was significantly increased in URSA mice and after rhHMGB1 intervention. (**J**,**K**) Flow cytometry detected the apoptotic cell (Annexin V$^+$PI$^+$) proportion in dMφ. It was significantly increased in URSA mice and after rhHMGB1 intervention.

(**L**,**M**) Flow cytometry detected pyroptosis (Caspase-1$^+$TUNEL$^+$) proportion in dMφ. It was significantly increased in URSA mice and after rhHMGB1 intervention. n = 7, $^{***}p < 0.001$ vs. NP group; $^{\#\#}p < 0.01$, $^{\#\#\#}p < 0.001$ vs. URSA group.

3.2 HMGB1 Promoted M1 Polarization of dMφ through TLR4/NF-κB Pathway

Elucidating HMGB1's regulatory effects and mechanism in dMφ polarization *in vitro*, primary dMφ were isolated, cultured, and purified from URSA mice as the main research object. By transfecting the OE-HMGB1 plasmid into dMφ, the HMGB1 protein level was notably enhanced (Fig. 2A,B). Overexpression of HMGB1 in dMφ significantly up-regulated TLR4 and NF-κB phosphorylation proteins, suggesting that HMGB1 might activate the TLR4/NF-κB axis (Fig. 2C,D). The percentage of M1 macrophage markers CD86 and CD80 positive cells in dMφ overexpressing HMGB1 increased significantly, while M2 macrophage marker CD206 positive cells decreased significantly, and there was no statistical difference in macrophage-specific marker F4/80 positive cell percentage (Fig. 2E–I), suggesting that the regulation of HMGB1 on dMφ polarization was phenotypically specific rather than affecting the total number. At the same time, overexpression of HMGB1 markedly enhanced inflammatory factor contents (Fig. 2J–L), and up-regulated iNOS protein level, while significantly reducing Arg1 expression (Fig. 2M,N). Overexpression of HMGB1 promoted the polarization of dMφ to M1 type. To verify whether HMGB1 is directly involved in the M1-like macrophage polarization process, Raw264.7 cells transfected with OE-HMGB1 were exposed to LPS+IFN-γ (classical M1 polarization inducer). OE-HMGB1 transfection or LPS+IFN-γ treatment alone could significantly increase M1-like macrophages (F4/80$^+$CD86$^+$CD206$^-$) and iNOS protein level, and significantly reduce M2-like macrophages (F4/80$^+$CD86$^-$CD206$^+$) and Arg1 protein, and combined treatment of the two showed a synergistic effect on the promotion of M1 polarization (Fig. 2O–S). Subsequently, to clarify the key roles of this axis in regulating dMφ polarization by HMGB1, this study used TLR4 inhibitor TAK-242 to intervene in dMφ transfected with OE-HMGB1. Compared with HMGB1 overexpression, TAK-242 markedly lessened TLR4 and NF-κB phosphorylation protein expressions (Fig. 3A,B), reduced CD86 positive cells, and raised CD206 positive cells (Fig. 3C–E). The above results confirmed that HMGB1 drives dMφ to M1 phenotype polarization through TLR4/NF-κB signal.

3.3 HMGB1 Triggered dMφ Pyroptosis via Activating NLRP3 Inflammasome

In order to verify whether HMGB1 triggers dMφ pyroptosis through activating NLRP3 inflammasome, NLRP3 agonist Nig and inhibitor MCC950 were introduced. HMGB1 overexpression could notably increase the positive rate of PI staining (Fig. 4A,B), indicating that overexpression of HMGB1 could promote the pore formation and membrane rupture of dMφ, which was a typical morphological feature of pyroptosis. At the same time, IL-1β and IL-18 concentrations were significantly raised (Fig. 4C,D), suggesting that HMGB1 promoted the maturation and release of inflammatory cytokines. Immunofluorescence found that HMGB1 overexpression facilitated ASC spot formation (Fig. 4E,F), suggesting NLRP3 inflammasome assembly and activation. NLRP3, Cleaved-Caspase-1, Cleaved-IL-1β, and Cleaved-GSDMD expressions were markedly increased after HMGB1 overexpression (Fig. 4G,H). The cleavage and up-regulation of these proteins together indicated that Caspase-1 was activated and GSDMD pores were formed, that is, the pyroptosis signaling pathway was completely initiated. Importantly, after the addition of MCC950, the above pyroptosis key indicators induced by HMGB1 overexpression were effectively reversed; the combined use of Nig showed a synergistic enhancement effect. In summary, under *in vitro* conditions, HMGB1 triggered dMφ pyroptosis via activating the NLRP3 inflammasome.

3.4 HMGB1 Activated NLRP3 by TLR4/NF-κB within dMφ In Vitro

In this study, on the basis of overexpression of HMGB1, the TLR4 inhibitor TAK-242 and the TLR4 agonist LPS were used for intervention. ASC spot formation in the OE-HMGB1 group was notably enhanced (Fig. 5A,B), and NLRP3 and Cleaved-Caspase-1 expressions were enhanced (Fig. 5C,D), which confirmed that HMGB1 overexpression effectively activated the NLRP3 inflammasome. After treatment with TAK-242, the NLRP3 inflammasome was significantly inhibited. Conversely, when LPS was used to co-activate the TLR4 pathway, a similar synergistic enhancement effect was observed with HMGB1 overexpression. In summary, HMGB1 activated NLRP3 inflammasome by targeting and depending on TLR4 receptor in dMφ *in vitro*.

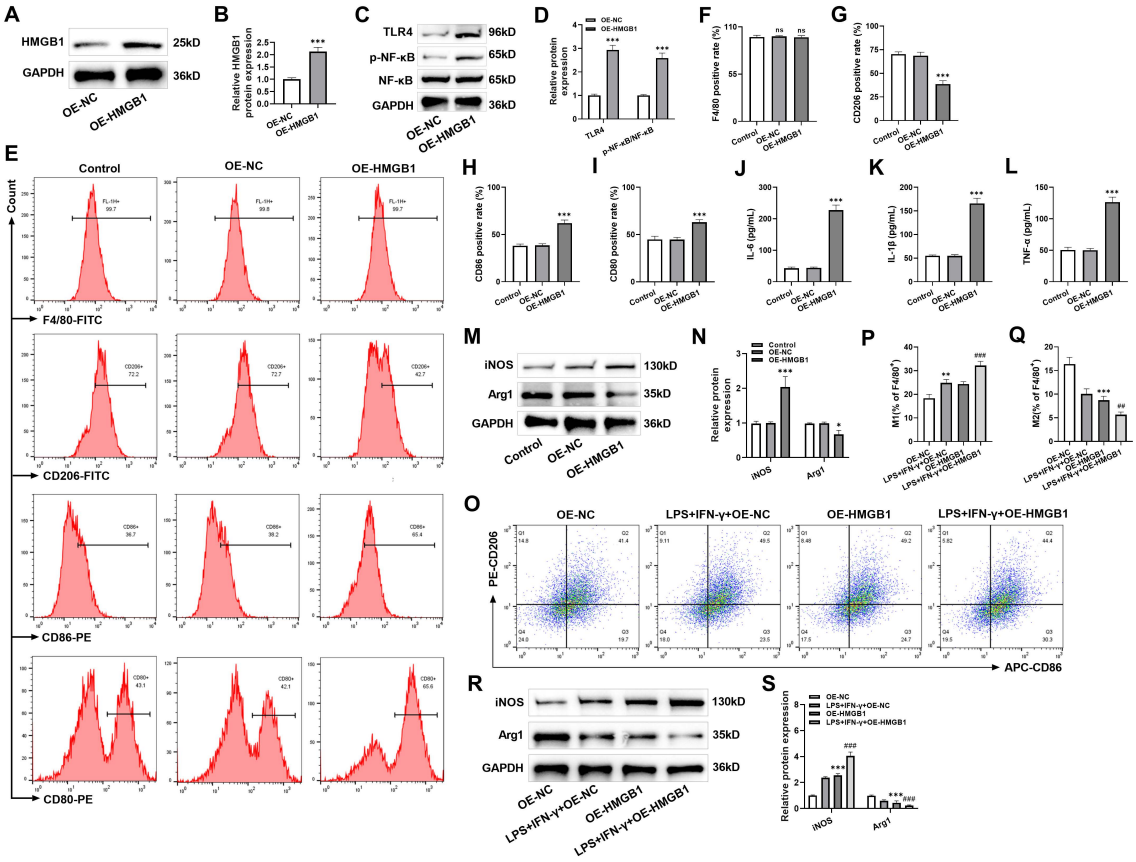

Figure 2: HMGB1 regulated the TLR4/NF-κB axis and promoted M1 polarization of dMφ. (**A**,**B**) OE-NC and OE-HMGB1 plasmids were transfected into dMφ, and HMGB1 proteins were analyzed. (**C**,**D**) Western blot analyzed TLR4 and p-NF-κB/NF-κB proteins, which were markedly enhanced after HMGB1 overexpression. (**E**–**I**) The expressions of F4/80, CD86, CD206 and CD80 were analyzed. HMGB1 overexpression markedly enhanced CD86 and CD80 positive cells, and decreased CD206 positive cells. (**J**–**L**) Inflammatory factor levels within dMφ were assessed, which were significantly increased after HMGB1 overexpression. (**M**,**N**) Western blot analyzed polarization markers. HMGB1 overexpression markedly increased the iNOS protein level and significantly decreased the Arg1 protein level. (**O**–**Q**) OE-NC and OE-HMGB1 plasmids were transfected into Raw264.7 cells, followed by treatment with LPS+IFN-γ. M1-like ($F4/80^+CD86^+CD206^-$) and M2-like ($F4/80^+CD86^-CD206^+$) macrophages was analyzed. HMGB1 overexpression or LPS+IFN-γ treatment significantly promoted M1 polarization. (**R**,**S**) Western blot analyzed polarization markers. HMGB1 overexpression or LPS+IFN-γ intervention markedly raised iNOS level and significantly lessened Arg1 protein level. n = 3, ns, not significant; $^{*}p < 0.05$, $^{**}p < 0.01$, $^{***}p < 0.001$ vs. OE-NC/LPS+IFN-γ+OE-NC group; $^{\#\#}p < 0.01$, $^{\#\#\#}p < 0.001$ vs. OE-HMGB1 group.

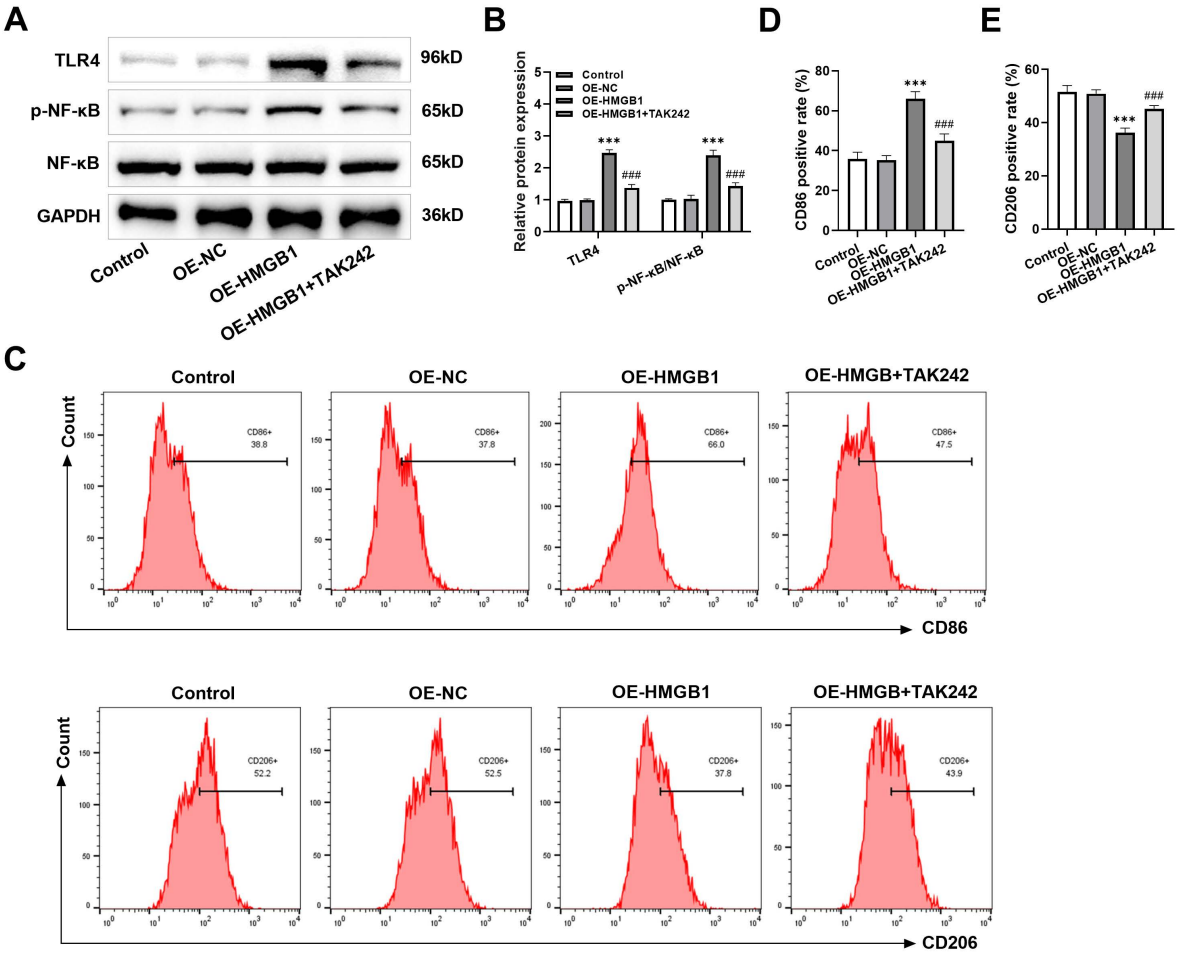

Figure 3: HMGB1 promoted M1 polarization of dMφ via the TLR4/NF-κB axis. (**A**,**B**) TLR4 inhibitor TAK-242 interfered with dMφ transfected with OE-HMGB1. TLR4/NF-κB signaling was detected, which was significantly decreased after TAK-242 intervention. (**C**–**E**) Flow cytometry analyzed M1 and M2 macrophage levels in macrophages. TAK-242 treatment significantly reduced CD86-positive cell rates and increased CD206-positive cell rates. n = 3, $^{***}p < 0.001$ vs. OE-NC group; $^{\#\#\#}p < 0.001$ vs. OE-HMGB1 group.

3.5 miR-216a-5p Inhibited TLR4/NF-κB/NLRP3 Signal within dMφ via Targeting HMGB1

In this study, we first predicted by bioinformatics analysis and cross-validated with multiple databases (TargetScan, miRWalk, and miRTarBase), and HMGB1 was a potential target for miR-216a-5p, and HMGB1 had a potential targeting relationship with miR-216a-5p (Fig. 6A). mimics markedly lessened WT-HMGB1 luciferase activity (Fig. 6B,C). In order to further clarify its function, we constructed miR-216a-5p knockdown and overexpression models, respectively. Its level was significantly decreased when inhibitor-miR-216a-5p treatment was applied, and markedly enhanced when mimics-miR-216a-5p treatment was applied (Fig. 6D), confirming that the two intervention models were successfully constructed. Subsequently, knockdown of miR-216a-5p notably up-regulated HMGB1, TLR4, NF-κB, and IκB phosphorylation proteins; its overexpression showed opposite effects (Fig. 6E–I). miR-216a-5p was simultaneously overexpressed in dMφ overexpressing HMGB1. Its overexpression could effectively reverse TLR4/NF-κB axis activation induced by HMGB1 overexpression (Fig. 6J–M). More importantly, to confirm that the observed phenotypic effect specificity was due to the targeted regulation of HMGB1 by miR-216a-5p rather than the off-target effect, we

co-transfected pHMGB1-NoUTR with overexpression of miR-216a-5p. The forced expressions of HMGB1, which were not regulated by miR-216a-5p, could restore HMGB1 down-regulation and TLR4/NF-κB signal suppression (Fig. 6N–R). The above results together proved that miR-216a-5p inhibited TLR4/NF-κB signal by inhibiting HMGB1 *in vitro*.

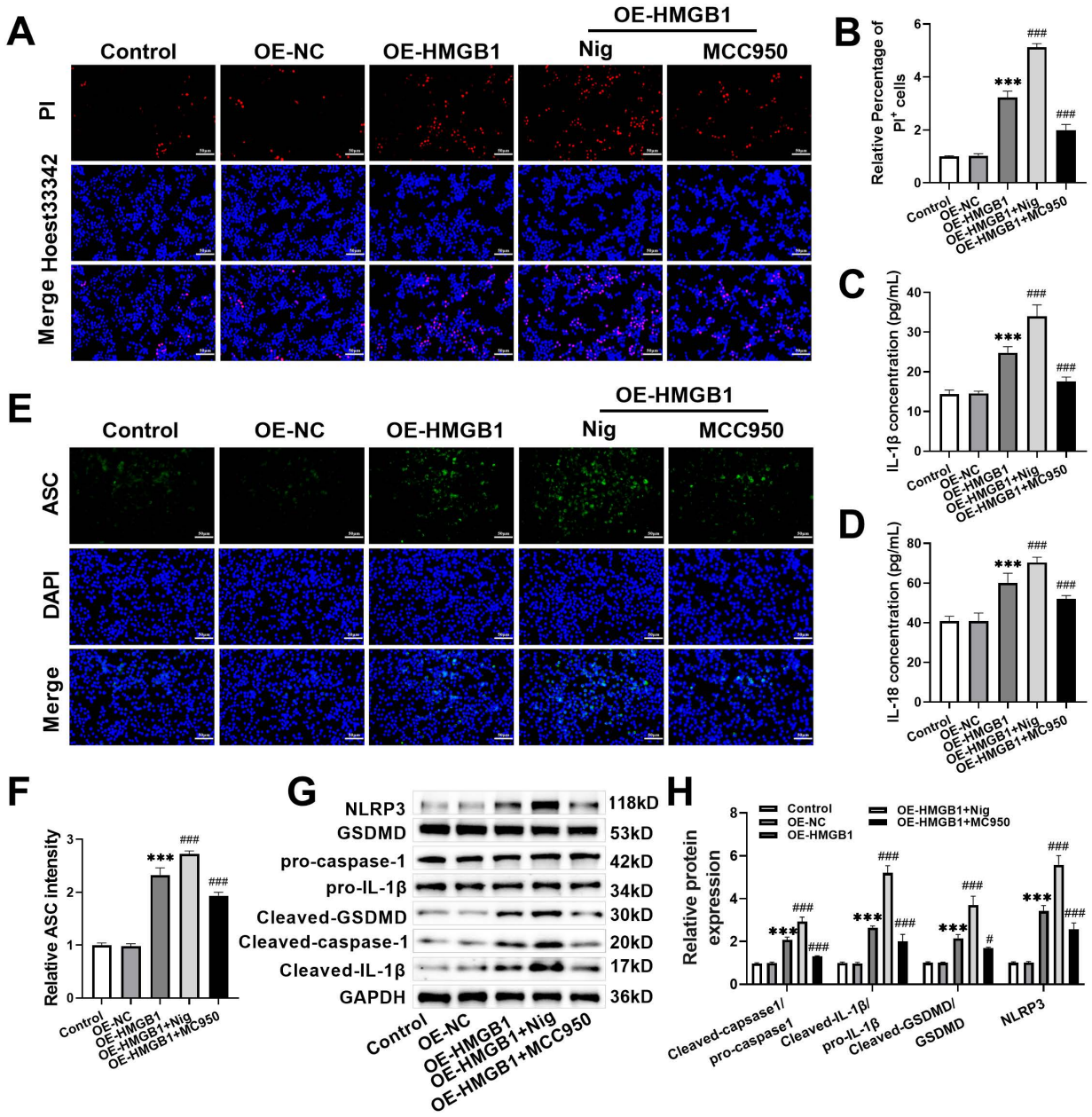

Figure 4: HMGB1 triggered dMφ pyroptosis via activating NLRP3. (**A**,**B**) PI staining to determine dMφ cell membrane rupture. Overexpression of HMGB1 significantly increased the positive rate of PI staining (×40, 50 μm). (**C**,**D**) IL-1β and IL-18 contents were assessed through ELISA, and they were markedly increased upon HMGB1 overexpression. (**E**,**F**) Immunofluorescence analyzed ASC expression. ASC fluorescence density was significantly increased after HMGB1 overexpression (×40, 50 μm). (**G**,**H**) Western blot assessed pyroptosis proteins. HMGB1 overexpression markedly increased pyroptosis. n = 3, $^{***}p < 0.001$ vs. OE-NC group; $^{\#}p < 0.05$, $^{\#\#\#}p < 0.001$ vs. OE-HMGB1 group.

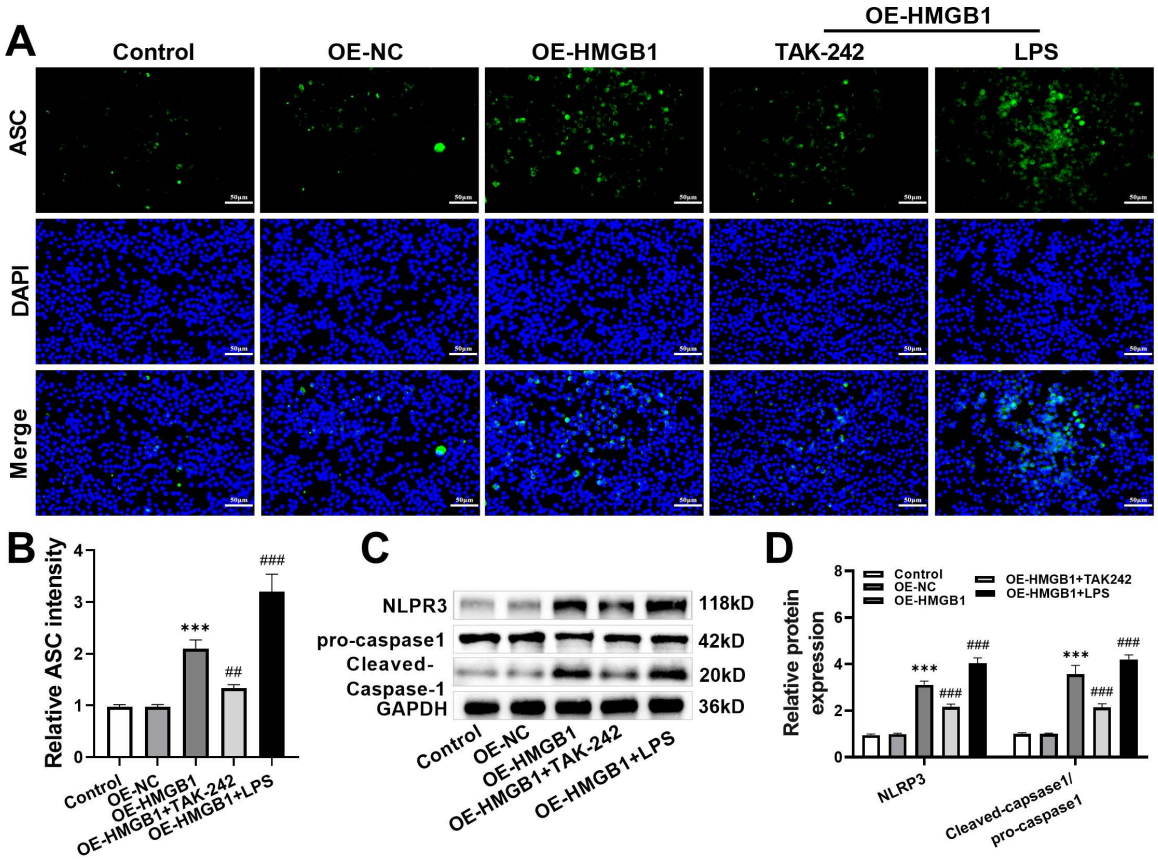

Figure 5: HMGB1 activated NLRP3 inflammasome through TLR4/NF-κB in dMφ. (**A**,**B**) Immunofluorescence analyzed ASC expression. ASC fluorescence density was significantly reduced after TAK-242 treatment (×40, 50 μm). (**C**,**D**) Western blot analyzed pyroptosis proteins. TAK-242 treatment significantly reduced NLRP3 and Cleaved-Caspase-1/pro-Caspase-protein levels. n = 3, $^{***}p < 0.001$ vs. OE-NC group; $^{\#\#}p < 0.01$, $^{\#\#\#}p < 0.001$ vs. OE-HMGB1 group.

3.6 miR-216a-5p Mitigatesd the Damage of HMGB1 on MFI of URSA

To verify miR-216a-5p's role in URSA, this research first confirmed that its expression in URSA decidual tissues was significantly down-regulated (Fig. 7A), suggesting that it is associated with MFI homeostasis. Subsequently, rhHMGB1, mimic-NC, and mimic-miR-216a-5p were used to intervene in URSA mice. Compared to rhHMGB1 intervention, mimic-miR-216a-5p treatment markedly declined HMGB1 protein level (Fig. 7B,C), the positive density of $CD68^+$/$TUNEL^+$ (macrophage apoptosis) (Fig. 7D,E), and the positive density of $CD68^+iNOS^+$ (M1 macrophages) (Fig. 7F,G) in decidual tissue of URSA mice. HE staining showed that mimic-miR-216a-5p treatment significantly lessened inflammatory damage within decidual tissue of URSA mice (Fig. 7H,I), confirming its protective effect on MFI tissue. In addition, its overexpression significantly reduced the number of M1-type dMφ ($CD11c^+CD206^-$) (Fig. 7J,K). Western blot results found that its overexpression markedly inhibited pyroptosis and TLR4/NF-κB/NLRP3 signal (Fig. 7L–O). Mimic-miR-216a-5p markedly declined the expression of HMGB1 (Fig. 7P,Q) and TLR4 (Fig. 7R,S) in $CD68^+$ macrophages and increased the fluorescence density of CD206 by immunofluorescence co-localization analysis. In summary, in the URSA mouse model, up-regulation of miR-216a-5p expression effectively antagonized HMGB1 pathogenic effects. This mechanism was to reduce the macrophage M1 polarization and pyroptosis and protect the MFI from inflammatory damage via targeting TLR4/NF-κB/NLRP3 signal.

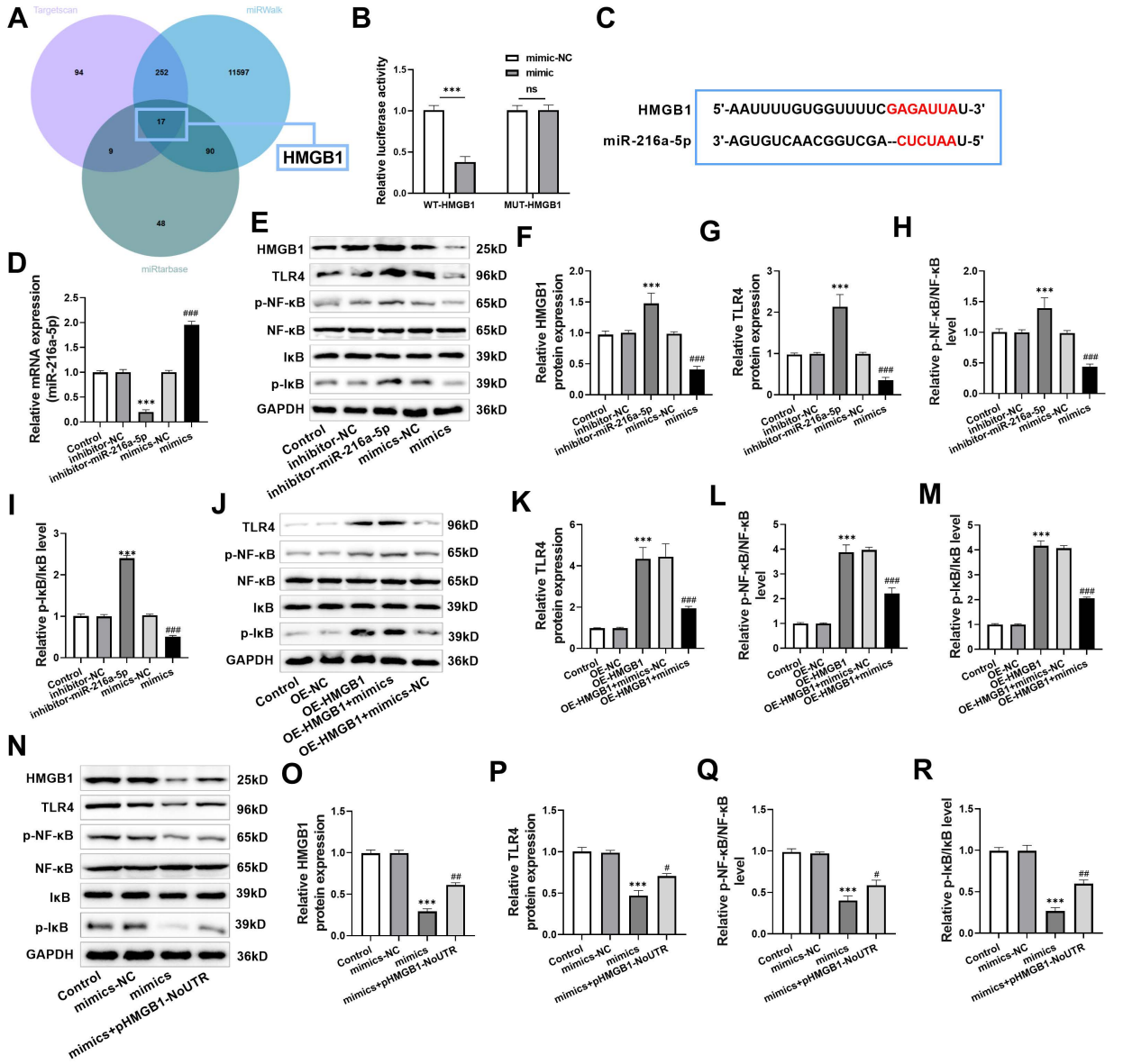

Figure 6: miR-216a-5p suppressed TLR4/NF-κB/NLRP3 signal within dMφ by targeting HMGB1. (**A**) Venn diagram. (**B**,**C**) Dual luciferase assay. Mimics markedly lessened WT-HMGB1 activity. (**D**) Inhibitor-NC, inhibitor-miR-216a-5p, mimics-NC, and mimics were transfected into dMφ. miR-216a-5p expression was examined using RT-qPCR. (**E**–**I**) TLR4/NF-κB signal was examined, which was significantly increased after miR-216a-5p knockdown. (**J**–**M**) TLR4/NF-κB signal was examined, which was markedly decreased upon miR-216a-5p overexpression. (**N**–**R**) Mimics and pHMGB1-NoUTR were transfected into dMφ. HMGB1 and TLR4/NF-κB signal expressions were analyzed. n = 3, ns, not significant; $^{***}p < 0.001$ vs. inhibitor-NC/OE-NC/mimics-NC group; $^{\#}p < 0.05$, $^{\#\#}p < 0.01$, $^{\#\#\#}p < 0.001$ vs. mimics-NC/OE-HMGB1+mimics-NC/mimics group.

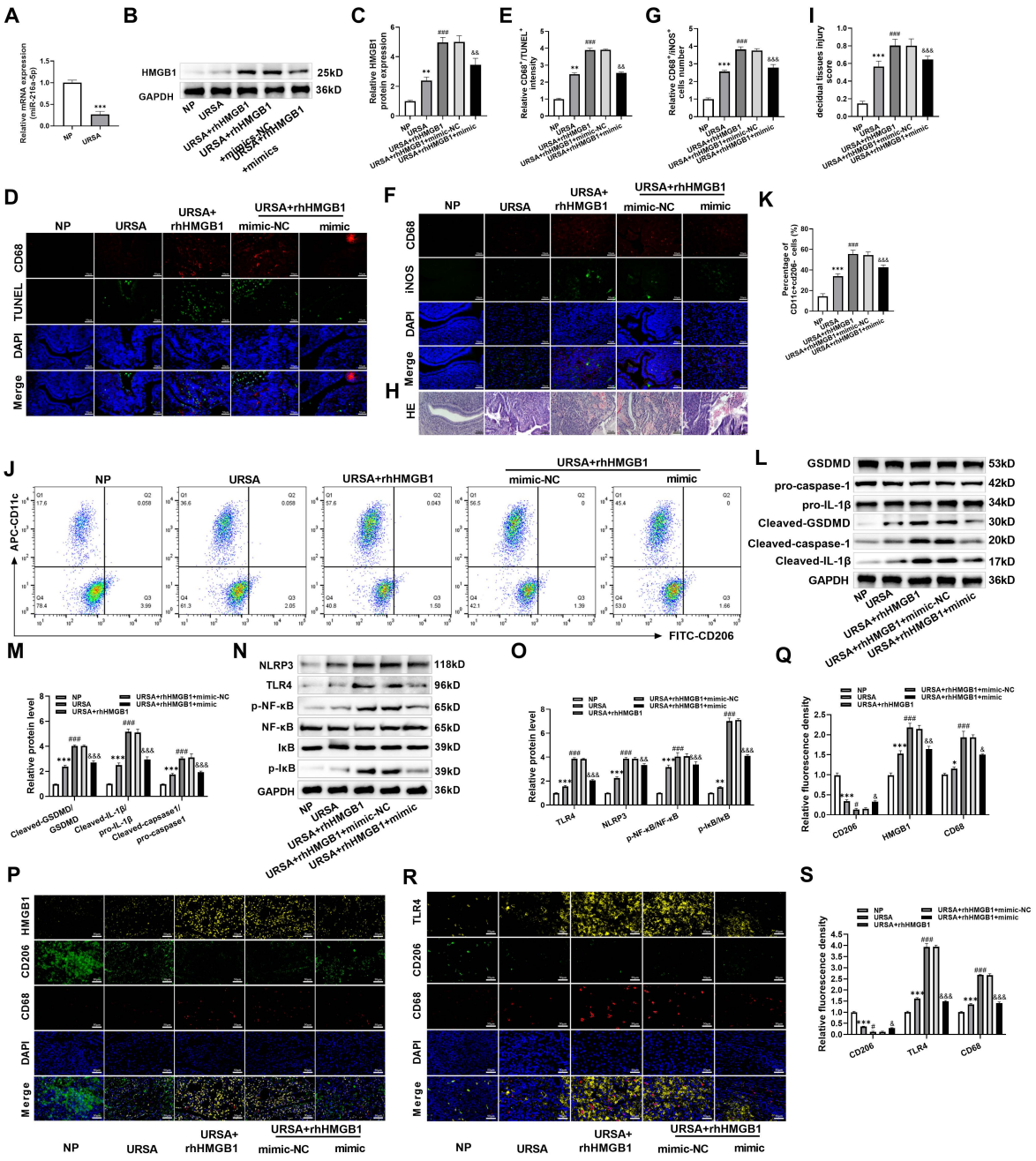

Figure 7: miR-216a-5p reduced the damage of HMGB1 in URSA mice. (**A**) miR-216a-5p expression in decidual tissue was detected, which was down-regulated in URSA mice. (**B**,**C**) URSA mice were treated with rhHMGB1, mimic-NC, and mimic-miR-216a-5p. HMGB1 protein level was detected by Western blot. mimic-miR-216a-5p treatment significantly reduced HMGB1 protein. (**D**,**E**) URSA mice were treated with rhHMGB1, mimic-NC, and mimic-miR-216a-5p. CD68/TUNEL immunofluorescence was used to detect macrophage apoptosis. mimic-miR-216a-5p treatment markedly lessened the positive density of $CD68^+$/$TUNEL^+$ in decidual tissue (×40, 50 μm). (**F**,**G**) CD68/iNOS immunofluorescence was used to detect M1 macrophages. mimic-miR-216a-5p treatment markedly lessened the positive density of $CD68^+iNOS^+$ in decidual tissue (×40, 50 μm). (**H**,**I**) HE staining evaluated the degree of inflammatory injury of decidual tissue in mice. miR-216a-5p overexpression markedly alleviated decidual tissue inflammatory injury (×40, 50 μm). (**J**,**K**) M1 type dMφ ($CD11c^+CD206^-$) proportion was analyzed, which was markedly decreased upon miR-216a-5p

overexpression. (**L**–**O**) Western blot detected pyroptosis markers and TLR4/NF-κB/NLRP3 signal axis, which were markedly declined after miR-216a-5p overexpression. (**P**–**S**) Immunofluorescence detected CD68, CD206, HMGB1, and TLR4 expressions. miR-216a-5p overexpression significantly lessened HMGB1 and TLR4 expression in $CD68^+$ macrophages and increased the fluorescence density of CD206 (×40, 50 μm). n = 7, $^*p < 0.05$, $^{**}p < 0.01$, $^{***}p < 0.001$ vs. NP group; $^{\#}p < 0.05$, $^{\#\#\#}p < 0.001$ vs. URSA group; $^{\&}p < 0.05$, $^{\&\&}p < 0.01$, $^{\&\&\&}p < 0.001$ vs. URSA+rhHMGB1+mimic-NC group.

4 Discussion

miR-216a-5p inhibited the TLR4/NF-κB/NLRP3 axis by targeting HMGB1 expression, reduced macrophage M1 polarization and pyroptosis, and finally alleviated the imbalance of the immune microenvironment in MFI of URSA (Fig. 8). Compared with previous studies that focused on a single molecule or pathway (such as the independent role of HMGB1 or TLR4), this study systematically clarified the role of the complete regulatory axis of 'miR-216a-5p → HMGB1 → TLR4/NF-κB → NLRP3 inflammasome → pyroptosis' in URSA for the first time, filling the cognitive gap in the field of upstream miRNA regulation of macrophage pyroptosis mechanism.

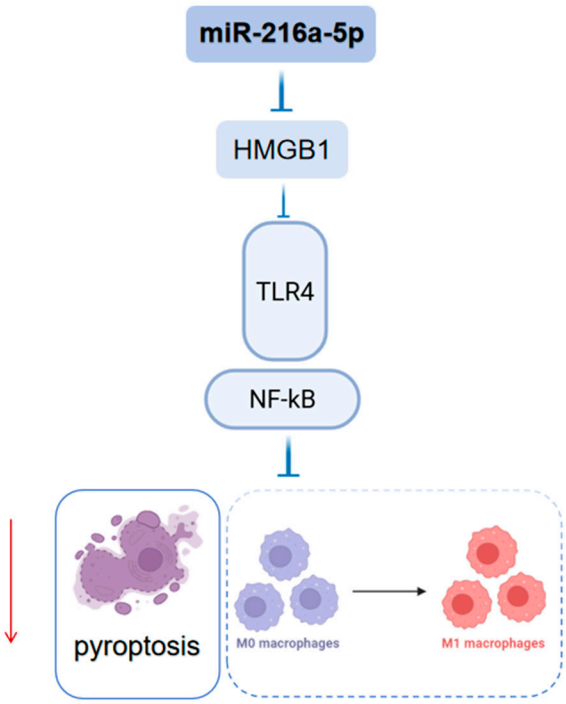

Figure 8: The mechanism of miR-216a-5p improving URSA by targeting HMGB1 to regulate the TLR4/NF-κB/NLRP3 signaling axis.

Due to the unknown etiology of URSA, the ability of doctors to develop effective prevention and treatment strategies is greatly limited, which aggravates the patient's uncertainty and stress [21]. As a key place for pregnancy maintenance, MFI affects the pregnancy process. Studies suggest that abnormal immune tolerance and inflammation within MFI are related to URSA [22]. In this study, we focused on HMGB1. By interacting with TLR4, HMGB1 triggers inflammatory pathways including NF-κB, enhances inflammatory factor release and white blood cell recruitment, and induces inflammation in MFI [23], playing a central role in pregnancy and immune regulation [24]. In the previous clinical study, Zhu et al. showed that HMGB1 was raised within URSA decidual tissues [12]. Xu et al. collected serum samples from 91

URSA patients and found that HMGB1 in URSA patients was higher [22]. This suggests that HMGB1 may be involved in URSA pathogenesis. The experimental data of this study further confirmed that HMGB1 overexpression aggravated the M1 polarization and pyroptosis of dMφ, resulting in increased MFI damage.

Macrophages are important immune cells at MFI; their phenotypic polarization is closely related to pregnancy outcomes. dMφ are vital for the formation and maintenance of MFI immune status. In the decidual tissue of early pregnancy, dMφ is transformed from M1 type to M2 type, which plays an anti-inflammatory and phagocytic role and regulates the local immune function of the decidua. This study found that in the URSA environment, dMφ was significantly shifted to the pro-inflammatory M1 phenotype, with this transition precisely controlled by the TLR4/NF-κB axis. HMGB1 overexpression activated this signaling pathway. After overexpression of HMGB1 in dMφ, the M1 phenotype was significantly increased. Importantly, TLR4 inhibitor TAK-242 successfully reversed TLR4/NF-κB activation and M1 phenotype up-regulation of dMφ induced by HMGB1 overexpression, which functionally verified the key role of this pathway in this process. This signaling pathway can regulate macrophage M1 polarization. When TLR4 is stimulated, it causes NF-κB activation and inflammatory mediator release associated with M1 phenotype [25,26]. In MFI of URSA, TLR4 and NF-κB expressions were also up-regulated [27]. And inhibiting this signaling can alleviate URSA and prevent abortion [28]. In summary, HMGB1 promotes M1 polarization of dMφ by the TLR4/NF-κB axis and participates in the URSA immune imbalance mechanism.

In addition to the phenotypic polarization of M1, pyroptosis in URSA pathogenesis has gradually emerged. The main feature of pyroptosis is cell membrane pore formation, causing increased cell membrane permeability and permeability dissolution, accompanied by inflammatory factor production. Pyroptosis is associated with NLRP3 inflammasome activation, the regulation of Caspase activity, and GSDM [29]. When NLRP3 is triggered by different external or internal damages, ASC and pro-Caspase-1 are initially recruited. The activated Caspase-1 facilitates inflammatory factor generation, as well as cleaves GSDMD protein, initiating pyroptosis [30,31]. The pyroptosis level in villous tissues of URSA is markedly increased, and inhibition of GSDMD and Caspase-1 can inhibit pyroptosis and reduce embryo absorption in URSA mice [32]. Chen et al. confirmed that ANXA6 overexpression promoted pyroptosis and up-regulated M1 macrophage polarization markers, while inhibiting NLRP3 rescued them [33]. Moreover, previous research confirmed that inhibition of HMGB1 can suppress pyroptosis and improve MFI destruction in URSA [12]. TLR4/NF-κB signaling not only drives M1 polarization but also provides the necessary starting signal for NLRP3 activation. NLRP3 inflammasome initiation depends on NF-κB activation [34,35]. The TLR4/NF-κB/NLRP3 signal is closely related to pyroptosis [36,37]. In this study, HMGB1 overexpression simultaneously activated the NLRP3 inflammasome and triggered pyroptosis, and TLR4 inhibitors could block this process. This is the first time to reveal the HMGB1-TLR4/NF-κB signal activation on macrophage pyroptosis within URSA.

The most important finding was to establish miR-216a-5p's protective role in URSA. miR-216a-5p was notably decreased in the URSA model mice. TargetScan, miRWalk, miRTarBase databases, and dual luciferase experiments suggest that miR-216a-5p has a targeted association with HMGB1, and miR-216a-5p inhibits HMGB1 expression. This study confirmed that miR-216a-5p directly targeted HMGB1 and inhibited its expression, thereby suppressing the TLR4/NF-κB axis. miR-216 a-5p overexpression can markedly reduce M1 macrophages and M1 dMφ in decidual tissue, alleviate the inflammatory damage, reduce the pyroptosis level, and significantly reverse the damage of MFI induced by HMGB1. These results suggest that it may inhibit the TLR4/NF-κB/NLRP3 axis by inhibiting HMGB1, reduce the M1 polarization and pyroptosis of dMφ, and improve the immune imbalance of MFI.

It should be noted that the expression regulation mechanism of miR-216a-5p itself is not further explored. The expression pattern of miRNA during early pregnancy is susceptible to the regulation of sex hormones and immune mediators [38,39]. Therefore, the significant reduction of miR-216a-5p within the URSA state observed in this study may be affected by the imbalance of hormone levels at MFI or the disorder of immunomodulatory factors. The above speculation needs to be further verified by *in vitro* cell experiments (such as decidual tissue cells treated with sex hormones or immune mediators) and *in vivo* experiments. In addition, traditional Chinese medicine has unique advantages in regulating maternal-fetal interface immune tolerance and treating URSA, among which kidney-tonifying Chinese medicine is widely used and has a definite curative effect. Studies have shown that the Bushen Antai recipe (BAR) can enhance immune tolerance and vascular remodeling at MFI, thereby reducing pregnancy loss [40]. BuShen HuoXue decoction (BSHXD) can interfere with autophagy and decidualization, and thus reduce URSA [41,42]. Chinese medicine for tonifying the kidneys and preventing miscarriage (such as dodder seed) can maintain pregnancy by affecting the function of trophoblast cells [43]. Whether these compounds or active ingredients exert their pregnancy-preserving effects by up-regulating miR-216a-5p expression or regulating the HMGB1/TLR4 axis is a transformation direction worthy of future exploration.

Of course, this research also has several limitations. The conclusion is mainly based on the mouse model, which needs to be further verified in human decidual tissue samples. Second, the etiology of URSA is extremely complex. In addition to macrophages, decidual NK cells, Treg cells, and other immune cells also play vital roles. Whether the miR-216a-5p/HMGB1 axis also affects the function of these cells remains to be further explored. In addition, the optimization of miRNA delivery *in vivo* is also the focus of future transformation research. The clinical application of miRNA therapy still faces challenges such as delivery systems, *in vivo* stability, and tissue targeting. Future research needs to explore safe and efficient *in vivo* delivery strategies (such as nanocarriers) and evaluate their long-term effects on pregnancy outcomes.

5 Conclusion

In summary, miR-216a-5p targeted HMGB1 and inhibited the TLR4/NF-κB/NLRP3 axis, thereby reducing the M1 polarization and pyroptosis of dMφ in URSA. This study systematically reveals the important role of miR-216a-5p/HMGB1/TLR4/NF-κB/NLRP3 axis in URSA pathogenesis, and offers novel theoretical frameworks for understanding the immune regulation imbalance at the MFI.

Acknowledgement: None.

Funding Statement: This research was funded by Jiaxing City Science and Technology Plan Project (No. 2023AY31023).

Author Contributions: The authors confirm contribution to the paper as follows: conceptualization, Weina Xu; methodology, Yi Xia; formal analysis, Qing Shen; investigation, Ling Ai; writing—original draft preparation, Weina Xu; writing—review and editing, Yi Xia; supervision, Weina Xu, Yi Xia; visualization, Yingye Lu; funding acquisition, Yingye Lu. All authors reviewed and approved the final version of the manuscript.

Availability of Data and Materials: The data supporting the findings of this study can be obtained from the corresponding author upon request.

Ethics Approval: This study was approved by Jiaxing Maternity and Child Health Care Hospital Ethics Committee (No. KY-2025-129).

Conflicts of Interest: The authors declare no conflicts of interest.

Abbreviations

NLRP3	nucleotide-binding oligomerization domain-like receptor protein 3
Caspase-1	cysteinyl aspartate-specific proteinase-1
pro-IL-1β	pro-inflammatory cytokine IL-1β
GSDMD	Gasdermin D
NF-κB	nuclear factor-κB
TNF-α	tumor necrosis factor-α
IL	interleukin
ASC	apoptosis-associated speck-like protein containing CARD
RSA	recurrent spontaneous abortion
URSA	unexplained recurrent spontaneous abortion
dMφ	decidual macrophages
HMGB1	high mobility group box 1
TLR4	toll-like receptor 4
ASPL	aspirin
FBS	fetal bovine serum
iNOS	inducible nitric oxide synthase
Arg1	Arginase 1
MFI	maternal-fetal interface

References

1. Zhou WJ, Yang HL, Mei J, Chang KK, Lu H, Lai ZZ, et al. Fructose-1, 6-bisphosphate prevents pregnancy loss by inducing decidual COX-2^{+} macrophage differentiation. Sci Adv. 2022;8(8):eabj2488. [CrossRef].
2. Tan Y, Wang J, Liu C, Wu S, Zhou M, Zhang Y, et al. KLF4 regulates trophoblast function and associates with unexplained recurrent spontaneous abortion. J Transl Med. 2024;22(1):922. [CrossRef].
3. Tang C, Hu W. The role of Th17 and Treg cells in normal pregnancy and unexplained recurrent spontaneous abortion (URSA): new insights into immune mechanisms. Placenta. 2023;142:18–26. [CrossRef].
4. Jiang X, Li L. Decidual macrophage: a reversible role in immunotolerance between mother and fetus during pregnancy. Arch Gynecol Obstet. 2024;309(5):1735–44. [CrossRef].
5. Duan H, Deng W, Kzhyshkowska J, Chen D, Zhang S. Macrophage at maternal-fetal interface: perspective on pregnancy and related disorders. Placenta. 2025. [CrossRef].
6. Shang Y, Wu S, Li S, Qin X, Chen J, Ding J, et al. Downregulation of EZH2 in trophoblasts induces decidual M1 macrophage polarization: a potential cause of recurrent spontaneous abortion. Reprod Sci. 2022;29(10):2820–8. [CrossRef].
7. Gao X, Hao Z, Du J, Zhang X, Yang S, Hu T, et al. Compromised adenosine-A2AR axis contributes to recurrent spontaneous abortion by promoting proinflammatory macrophage polarization. Int Immunopharmacol. 2025;158:114838. [CrossRef].
8. Zhao Y, Miao C, Wang R, Chen Y, Ren N, Ma J, et al. Jianpi Antai formula prevents miscarriage by repressing M1 polarization of decidual macrophages through ubiquitination of NLRP3 mediated by MARCH7. J Ethnopharmacol. 2024;324:117796. [CrossRef].
9. Wang B, Yang Y, Ye J, Han X, Yang L, Huang Y, et al. GRIM-19 deficiency promotes macrophage polarization to the M1 phenotype partly through glycolysis in unexplained recurrent spontaneous abortion. Biol Reprod. 2024;110(4):739–49. [CrossRef].
10. He Y, Wang L, Tang R, Jin H, Liu B, Chen S, et al. Common mental disorders and risk of spontaneous abortion or recurrent spontaneous abortion: a two-sample Mendelian randomization study. J Affect Disord. 2024;354:258–66. [CrossRef].
11. Wang J, Zhu D, Yin J, Ma C, Peng X, Zou H, et al. Upregulated HMGB1 levels in maternal-fetal interface of patients with unexplained recurrent spontaneous abortion from different sources. J Matern Fetal Neonatal Med. 2022;35(25):6542–9. [CrossRef].

12. Zhu D, Zou H, Liu J, Wang J, Ma C, Yin J, et al. Inhibition of HMGB1 ameliorates the maternal-fetal interface destruction in unexplained recurrent spontaneous abortion by suppressing pyroptosis activation. Front Immunol. 2021;12:782792. [CrossRef].
13. Wang J, Nuray U, Yan H, Xu Y, Fang L, Li R, et al. Pyroptosis is involved in the immune microenvironment regulation of unexplained recurrent miscarriage. Mamm Genome. 2024;35(2):256–79. [CrossRef].
14. Ashrafizadeh M. Cell death mechanisms in human cancers: molecular pathways, therapy resistance and therapeutic perspective. J Cancer Biomol Ther. 2024;1(1):17–40. [CrossRef].
15. Zhao M, Zheng Z, Zhang P, Xu Y, Zhang J, Peng S, et al. IL-30 protects against sepsis-induced myocardial dysfunction by inhibiting pro-inflammatory macrophage polarization and pyroptosis. iScience. 2023;26(9):107544. [CrossRef].
16. Qi X, Ding Y, Zheng J, Geng X, Zhang J, Xu Y. Hsa-miR-194-5p regulates TRAF6-mediated M1 macrophage apoptosis in recurrent spontaneous abortion. J Mol Histol. 2025;56(3):166. [CrossRef].
17. Zhou Z, Liu F, Ma M, Li R, Sun W, Wang Q. Targeting HMGB1-TLR4 signaling by miR-216a-5p elevation alleviates the inflammatory behavioral hypersensitivity. Neurosci Lett. 2021;759:136043. [CrossRef].
18. Xue L, Hu M, Zhu Q, Li Y, Zhou G, Zhang X, et al. GRg1 inhibits the TLR4/NF-kB signaling pathway by upregulating miR-216a-5p to reduce growth factors and inflammatory cytokines in DR. Mol Biol Rep. 2023;50(11):9379–94. [CrossRef].
19. Qian W, Huang L, Xu Y, Lu W, Wen W, Guo Z, et al. Hypoxic ASCs-derived exosomes attenuate colitis by regulating macrophage polarization via miR-216a-5p/HMGB1 axis. Inflamm Bowel Dis. 2023;29(4):602–19. [CrossRef].
20. Ma Y, Wang Y, Chen R, Wang Y, Fang Y, Qin C, et al. Exosomal transfer of pro-pyroptotic miR-216a-5p exacerbates anthracycline cardiotoxicity through breast cancer-heart pathological crosstalk. Signal Transduct Target Ther. 2025;10(1):157. [CrossRef].
21. Yao Y, Ye Y, Chen J, Zhang M, Cai X, Zheng C. Maternal-fetal immunity and recurrent spontaneous abortion. Am J Reprod Immunol. 2024;91(5):e13859. [CrossRef].
22. Xu X, Wang J, Zhu D, Yin J, Liu J, Wu X, et al. Low-dose aspirin protects unexplained recurrent spontaneous abortion via downregulation of HMGB1 inflammation activation. Front Endocrinol. 2022;13:914030. [CrossRef].
23. Saito Reis CA, Padron JG, Norman Ing ND, Kendal-Wright CE. High-mobility group box 1 is a driver of inflammation throughout pregnancy. Am J Reprod Immunol. 2021;85(1):e13328. [CrossRef].
24. Liu J, Wu Z, Guo S, Zhang T, Ma X, Jiang K, et al. IFN-τ attenuates LPS-induced endometritis by restraining HMGB1/NF-κB activation in bEECs. Inflammation. 2021;44(4):1478–89. [CrossRef].
25. Liu B, Yu J, Zhang J, Ye W, Yao J. TLR4/NF-κB-mediated M1 macrophage polarization contributes to the promotive effects of ETS2 on ulcerative colitis. Eur J Med Res. 2025;30(1):668. [CrossRef].
26. Fang R, Zhou R, Ju D, Li M, Wang H, Pan L, et al. Zhen-wu-tang protects against myocardial fibrosis by inhibiting M1 macrophage polarization via the TLR4/NF-κB pathway. Phytomedicine. 2024;130:155719. [CrossRef].
27. Zou H, Yin J, Zhang Z, Xiang H, Wang J, Zhu D, et al. Destruction in maternal-fetal interface of URSA patients via the increase of the HMGB1-RAGE/TLR2/TLR4-NF-κB signaling pathway. Life Sci. 2020;250:117543. [CrossRef].
28. Huang C, Cheng EF, Ni J, Lyu Y. Baicalein prevents pregnancy loss by maintaining regulatory T cell activation through inhibition of the TLR4/NF-κB signaling pathway. Placenta. 2025;165:120–6. [CrossRef].
29. Li Z, Ji S, Jiang ML, Xu Y, Zhang CJ. The regulation and modification of GSDMD signaling in diseases. Front Immunol. 2022;13:893912. [CrossRef].
30. Wang Y, Li Y, Zhang W, Yuan Z, Lv S, Zhang J. NLRP3 inflammasome: a novel insight into heart failure. J Cardiovasc Transl Res. 2023;16(1):166–76. [CrossRef].
31. Zhong Y, Li XY, Liang TJ, Ding BZ, Ma KX, Ren WX, et al. Effects of NLRP3 inflammasome mediated pyroptosis on cardiovascular diseases and intervention mechanism of Chinese medicine. Chin J Integr Med. 2024;30(5):468–79. [CrossRef].
32. Zhu X, Xu K, Ai S, Zhang Y, Chu C, Wei R, et al. miR-126-5p protects from URSA via inhibiting Caspase-1-dependent pyroptosis of trophoblast cells. Cell Mol Life Sci. 2025;82(1):204. [CrossRef].
33. Chen X, Li XY, Ma XQ, Zhang Y, Song QL, Yang J. ANXA6 overexpression causes abnormal decidual macrophage-trophoblast crosstalk in recurrent spontaneous abortion. Int J Biol Sci. 2025;21(12):5206–22. [CrossRef].

34. Li Z, Chi H, Zhu W, Yang G, Song J, Mo L, et al. Cadmium induces renal inflammation by activating the NLRP3 inflammasome through ROS/MAPK/NF-κB pathway *in vitro* and *in vivo*. Arch Toxicol. 2021;95(11):3497–513. [CrossRef].
35. Liu YR, Wang JQ, Li J. Role of NLRP3 in the pathogenesis and treatment of gout arthritis. Front Immunol. 2023;14:1137822. [CrossRef].
36. Wang K, Yang J, Deng J, Wang A, Chen G, Lin D. Pinocembrin reduces pyroptosis to improve flap survival by modulating the TLR4/NF-κB/NLRP3 signaling pathway. Biochim Biophys Acta Mol Basis Dis. 2025;1871(3):167710. [CrossRef].
37. Zhou X, Xing S, Zhang L, Lu J, Li D, Wang Y, et al. Amniotic mesenchymal stem cells attenuate diabetic cardiomyopathy by inhibiting pyroptosis via modulation of the TLR4/NF-κb/NLRP3 pathway. Front Cell Dev Biol. 2025;13:1631973. [CrossRef].
38. Wang Y, Ji Z, Yao N, Hu X, Zhou R, Wang X, et al. The role of microRNAs in the regulation of critical genes and signalling pathways that determine endometrial receptivity. Zygote. 2024;32(4):261–70. [CrossRef].
39. Gan J, Gu T, Yang H, Ao Z, Cai G, Hong L, et al. Non-coding RNAs regulate spontaneous abortion: a global network and system perspective. Int J Mol Sci. 2022;23(8):4214. [CrossRef].
40. Liu Z, Geng Y, Huang Y, Hu R, Li F, Ding J, et al. Bushen Antai recipe alleviates embryo absorption by enhancing immune tolerance and angiogenesis at the maternal-fetal interface via mobilizing MDSCs in abortion-prone mice. Phytomedicine. 2024;123:155164. [CrossRef].
41. Feng X, Jiang S, Leung W, Wang L, Gober HJ, Chen L, et al. BuShen HuoXue decoction promotes decidual stromal cell proliferation via the PI3K/AKT pathway in unexplained recurrent spontaneous abortion. Evid Based Complement Alternat Med. 2020;2020(1):6868470. [CrossRef].
42. Zhao X, Jiang Y, Ren J, Wang Y, Zhao Y, Feng X. Deciphering the mechanism of Bushen Huoxue decotion on decidualization by intervening autophagy via AMPK/mTOR/ULK1: a novel discovery for URSA treatment. Front Pharmacol. 2022;13:794938. [CrossRef].
43. Zheng W, Lei M, Yao Y, Zhan J, Zhang Y, Zhou Q. Mechanisms underlying the therapeutic effects of *Semen cuscutae* in treating recurrent spontaneous abortion based on network pharmacology and molecular docking. Front Mol Biosci. 2024;11:1282100. [CrossRef].